Original Article

MOLECULAR METABOLISM

Berardinelli–Seip congenital lipodystrophy 2/ SEIPIN determines brown adipose tissue maintenance and thermogenic programing

Hongyi Zhou, Cheng Xu, Hakjoo Lee, Yisang Yoon, Weiqin Chen*

ABSTRACT

Objective: Understanding the mechanisms that control brown adipose tissue (BAT) mass and functionality is crucial for our understanding of how the disruption of energy homeostasis leads to obesity. Bernerdinali Seip Congenital Lipodystrophy (BSCL) type 2 (BSCL2, a.k.a. SEIPIN), a lipodystrophy-associated protein, has been shown to not be required for brown adipogenesis, but it has been shown to be essential for perinatal BAT development. However, its role in mature BAT maintenance and thermogenic programing remains poorly understood.

Methods: We subjected *Bscl2*$^{f/f}$ and *Bscl2*$^{UCP1\text{-}BKO}$ (BKO) mice with a brown adipose-specific loss of BSCL2 through UCP1 promoter-driven Cre to environmental, pharmacological and diet interventions to challenge BAT functionality and reprogramming. We carried out physiological, molecular and transcriptomic analyses of BAT.

Results: The deletion of BSCL2 in mature brown adipocytes increased sympathetic nervous system-independent cAMP/protein kinase A (PKA) signaling in BAT. Such activation reduced BAT triglyceride content and mass and was sufficient to reduce plasma triglyceride, but not enough to combat thermoneutral and high fat diet-induced obesity. Surprisingly, BKO mice displayed an impaired response to acute and chronic cold challenges despite cAMP/PKA activation. When subjected to chronic cold exposure or the administration of a β3-adrenergic agonist, CL 316,243, BKO mice failed to induce BAT recruitment and underwent dramatic brown adipocyte loss. Transcriptomic analysis revealed pathological BAT remodeling with inflammation and fibrosis, which was further exacerbated by a chronic thermogenic challenge in BKO mice. Mechanistically, we found abnormal mitochondrial shapes and function in BAT of BKO mice housed at 21 °C; as well as mitochondrial DNA depletion and necroptotic-mediated brown adipocyte death after chronic thermogenic insult.

Conclusion: BSCL2-mediated lipid catabolism within BAT is crucial for mature brown adipocyte function and survival both during times of activation and quiescence. BSCL2 is an important regulator of mature brown adipocyte mitochondrial metabolism, necroptosis and thus adaptive thermogenesis.

Keywords BSCL2; Lipodystrophy; Brown adipose tissue; Thermogenesis; Obesity; Metabolism

1. INTRODUCTION

Brown adipose tissue (BAT) is a unique metabolic organ that actively oxidizes lipids and glucose through uncoupled mitochondrial respiration to produce heat and maintain body temperature, that is, non-shivering thermogenesis (NST) [1]. Functional BAT decreases with age and in obesity and diabetes [2–5]. A growing body of evidence suggests that interventions to increase BAT mass/activity could potentially promote adaptive thermogenesis to reduce adiposity and improve glucose and lipid parameters in obesity [6–9]. Thus understanding BAT maintenance and function is of high clinical relevance.

Cold activates the sympathetic nervous system (SNS) to increase BAT oxidative metabolism for the production of heat required for survival [1]. Activated SNS releases norepinephrine (NE), which acts through β-adrenergic receptors (β-ARs) to rapidly induce cAMP/protein kinase A (PKA)-mediated hydrolysis of intracellular triglyceride (TG) store via activation of hormone sensitive lipase (HSL) and adipose triglyceride lipase (ATGL) [10]. Non-esterified fatty acids (NEFAs) within BAT serve dual roles by undergoing beta-oxidation to support thermogenesis and by allosterically activating uncoupling protein 1 (UCP1) to generate heat instead of ATP synthesis in the mitochondria [1]. Impaired thermogenesis is observed in mice deficient for genes associated with fatty acid oxidation [11,12]. Intracellular TG stores are the likely primary energy source for activated BAT [13,14], although a recent study demonstrates that ATGL-mediated TG lipolysis in BAT is not a prerequisite for cold-induced NST in vivo [15]. Sustained activity of BAT in a cold environment requires utilization of circulating NEFAs and TG-rich lipoproteins (TRLs). BAT thermogenic programing and plasticity is also an important contributor to long-term cold tolerance. Cold acclimation triggers BAT hyperplasia, involving proliferation and differentiation of precursor cells, and hypertrophy of mature brown adipocytes [16]. Mitochondrial biogenesis and increased synthesis of UCP-1 are hallmarks of the thermogenic recruitment process [17], but the role of BAT

Department of Physiology, Medical College of Georgia at Augusta University, Augusta, GA 30912, USA

*Corresponding author. Fax: +706 721 7299. E-mail: wechen@augusta.edu (W. Chen).

Received December 25, 2019 • Revision received February 18, 2020 • Accepted February 25, 2020 • Available online 4 March 2020

https://doi.org/10.1016/j.molmet.2020.02.014

lipid metabolism in structure, function and plasticity of BAT under conditions of metabolic stress is not well defined.

Berardinelli—Seip Congenital Lipodystrophy 2 (BSCL2, a.k.a. SEIPIN) is an endoplasmic reticulum (ER) membrane protein, mutations of which are associated with human Bernerdinali Seip Congenital Lipodystrophy (BSCL) type 2 disease [18—22]. This protein is highly expressed in the testis, brain and adipose tissue [19—22]. Global *Bscl2*-deficient (*Bscl2*$^{-/-}$) mice recapitulate human BSCL2 disease, exhibiting congenital lipodystrophy and severe insulin resistance [23—25]. Various molecular functions of BSCL2 have been proposed, which range from regulating lipid droplet (LD) biogenesis [26—31] to ER calcium signaling and mitochondrial metabolism [32,33]. Human BSCL2 assembles as an undecamer and directly binds to anionic phospholipids [34]; whereas *Drosophila* BSCL2 forms dodecamers and plays a role in lipid transfer and LD formation [35]. BSCL2 has been shown to interact with 1-acylglycerol-3-phosphate O-acyltransferase 2 (AGPAT2) [36], LIPIN1 [37], glycerol-3-phosphate acyltransferase 3 (GPAT3) [31] and, most recently, Promethin [38,39]. However, these data were mainly generated in non-adipocyte cells in vitro, and the relevance to mature adipocytes in vivo remains unclear.

We have demonstrated that BSCL2 regulates cAMP/PKA-mediated lipolysis, which is essential for white adipocyte differentiation and maintenance [23,40]. Rodent BAT has the highest level of *Bscl2* mRNA expression of all adipose tissues [19]. It is not required for brown adipocyte differentiation [41,42], but deletion of BSCL2 promotes cAMP/PKA signaling coupled with enhanced fatty acid oxidation and uncoupling in cultured brown adipocytes and BAT homogenates, mimicking sympathetic nerve activation [40,42]. Lipodystrophic *Bscl2*$^{-/-}$ mice and *Bscl2*$^{Ad\text{-}mKO}$ mice with acquired deletion of BSCL2 in both white and brown adipocytes display mild BAT atrophy [40,41]. These mice are sensitive to acute cold stimulation during fasting due to a lack of white adipose tissue (WAT) ([41] and own observations), and are able to acclimate to the cold through a compensatory hyperphagia [40,41]. The deletion of BSCL2 in Myf5+ progenitor cells potentiates cAMP/PKA signaling during postnatal BAT development, which results in severe BAT atrophy yet elevated white adiposity [42]. Surprisingly, the BAT-less *Bscl2*$^{Myf\text{-}BKO}$ mice are able to maintain thermogenesis under both acute and chronic cold stress [42]. Whether BSCL2 plays a cell-autonomous role in regulating mature brown adipocyte thermogenic function and tissue remodeling in response to a thermogenic challenge has not been investigated.

In this study, we specifically deleted BSCL2 in mature UCP1 — expressing brown adipocytes to determine the importance of BSCL2 in BAT maintenance and thermogenic programming. We confirmed an essential role for BSCL2 in regulating SNS — independent cAMP/PKA signaling in mature brown adipocytes, which was able to protect against circulating hypertriglyceridemia but not thermoneutral or high fat diet-induced obesity. However, deletion of BSCL2 depleted BAT TG storage and reduced BAT mass, which rendered animals catastrophic when subjected to disparate thermogenic stimuli including cold exposure or β3-adrenergic agonist CL 316,243 (CL) treatment. Our data demonstrate that reduced BAT TG and mass contribute to defective thermogenesis despite activation of cAMP/PKA signaling and underscore the indispensable role of BSCL2 in maintaining brown adipocyte function and fate.

2. MATERIALS AND METHODS

2.1. Animals and treatments

Brown adipocyte-specific *Bscl2* knockout mice (*Bscl2*$^{UCP1\text{-}BKO}$, a.k.a. BKO) mice were obtained by breeding *Bscl2*$^{f/f}$ mice [23] with transgenic mice expressing UCP1 — driven Cre recombinase [B6.FVB-Tg(UCP1-Cre)1Evdr/J, kindly provided by Dr. Evan D. Rosen, Harvard Medical School]. Experiments were performed in male mice with major findings repeated in female mice. Representative data from male mice were presented. If not specified, all mice were housed in the central animal facility with room temperature controlled at 21 °C, and an artificial 12 h:12 h light: dark cycle (lights on at 06:00 am). All procedures involving animals were approved by the IACUC at Augusta University (IACUC Protocol # 2012-0462).

Fat and lean masses were measured using a Bruker small animal NMR system (Bruker minispec LF90II). Energy expenditure, respiratory exchange ratio (RER), food intake and locomotor activity were measured using a comprehensive laboratory animal monitoring system (CLAMS: Columbus Instruments, Columbus, OH, USA). Mice were acclimated to the CLAMS for 2 days before making measurements for 2 days. For glucose tolerance tests (GTT), 6 h-fasted mice received i.p. injections of 1.5 g glucose/kg body weight. Blood glucose levels were measured by the One-touch Ultra glucose meter before and at 15, 30, 60 and 120 min after glucose injection. For insulin tolerance tests (ITT), 6 h-fasted mice were injected i.p. with 0.75 U/kg body weight human insulin (Humulin, Novo Nordisk). Blood glucose levels were measured before and at 15, 30, 60, 90 and 120 min after injection. For insulin signaling in BAT, 6 h-fasted mice were i.p. injected with 1.0 U/kg body weight human insulin. BAT was dissected 15 min after insulin injection.

For temperature acclimation studies, mice were housed in an environmental chamber at 30 °C (group housed with normal chow diet) or at 4 ± 1 °C (individually housed in the presence or absence or food) under a controlled 12 h/12 h light—dark cycle. Rectal temperatures were measured using a BAT-12 thermometer (Physitemp). Mice treated with a β-agonist received i.p. injections of vehicle (PBS) or CL 316,243 (Sigma-Aldrich, 1 mg/kg/day) daily for 5 consecutive days. For the diet study, male control and BKO mice were fed a 60% high fat diet (HFD, Research Diets; D12492) for 12 weeks starting at 6-weeks of age. Body weights were recorded on a weekly base. Ad libitum-fed or 4 h-fasted mice were sacrificed by cervical dislocation.

2.2. Plasma parameters

Blood was collected from the tail vein of mice in Microvette CB300 LH K2E tubes (Sarstedt). Plasma NEFA and TG levels were measured by colorimetrical analyses using the WAKO NEFA analysis kit (NEFA-HR(2); Wako Pure Chemical Industries) and the Infinity™ triglycerides kit, (Thermo Fisher Scientific), respectively.

2.3. Histology, immunohistochemistry, trichrome staining and transmission electron microscopy (TEM)

Tissues were formalin fixed, paraffin embedded, sectioned and stained with Hematoxylin—eosin (H&E). Galectin 3 immunohistochemistry was performed as previously described [42]. Trichrome staining was performed using a Trichrome Staining Kit (Abcam, ab150686) according to the manufacturers' directions. For TEM, BAT samples were collected, processed and imaged on a JEM 1230 transmission electron microscope (JEOL USA Inc., Peabody, MA) as previously described [43].

2.4. RNA-seq and data analysis

RNA was isolated from BAT using Trizol™. cDNA libraries generations, next generation sequencing, and data analyses were performed by the Integrated Genomics Resource Center at Augusta University as previously described in detail [40]. Differential gene expression was assessed with DESeq2 using HOMER's getDiffExpression.pl with the

parameters — adj. $P < 0.05$ and −log2 fold 1.0 [for 2-fold differently expressed genes (DEGs)]. For all the DEGs, the Z-scaled log2 [TPM] (transcript per kilobase million) values were plotted and colored. Based on the 99 DEGs, enrichment of the Gene Ontology (GO) biological process terms was analyzed using the GOEAST program [44]. The R/Bioconductor package heatmap3 was used to display heatmaps for GO term with a Benjamini–Hochberg false-discovery rate adjusted *P*-value less than or equal to 0.05. Data have been submitted to the GEO database with the following accession number: GSE145070.

2.5. Tissue TG, DNA and mitochondrial DNA quantification

Tissues were homogenized in standard PBS buffer followed by lipid extraction and determination of TG concentration using Infinity™ triglycerides kit (Thermo Fisher Scientific) as previously described [45]. Data were normalized to starting tissue weight. Total DNA was extracted from BAT. Nuclear DNA (nDNA) was quantified by RT-PCR of nDNA-encoded hexokinase 2 (*Hk2*) intron 9. A known amount of mouse nuclear DNA was used to generate a standard curve for calculation. Data were presented as total amounts per BAT depot. Mitochondrial DNA (mtDNA) content was analyzed by RT-PCR of mtDNA-encoded 16s RNA (*MT-Rnr2*) to nDNA-encoded hexokinase 2 (*Hk2*) intron 9 as described previously [42].

2.6. Mitochondrial bioenergetic analysis

Freshly collected BAT were minced and homogenized in a glass Teflon douncer followed by mitochondria isolation and immediate analysis in a Seahorse XF24 Analyzer (Agilent Technologies, Inc.) as previously described [46]. Briefly, mitochondria were suspended in MAS buffer (220 mM mannitol, 70 mM sucrose, 10 mM KH2PO4, 5 mM MgCl2, 2 mM HEPES, 1.0 mM EGTA, 1 mM EDTA, 0.2% BSA, pH 7.2) containing 10 mM succinate and 2 μM rotenone. Next, 3 μg mitochondria were seeded per well by centrifugation. The coupling assays were performed by measuring oxygen consumption rates (OCR) after sequential addition of 4 mM adenosine 5′-diphosphate (ADP) (Complex V substrate), 2.5 μg/ml oligomycin (Complex V inhibitor), 4 μM carbonyl cyanide 4-(trifluoromethoxy)phenylhydrazone (FCCP) (mitochondrial uncoupler for maximal respiration), and 4 μM antimycin A (Complex III inhibitor). Coupled respiration was the oligomycin-sensitive OCR while uncoupled was the OCR difference between oligomycin and antimycin A additions.

2.7. Quantitative real-time RT-PCR analysis

Total RNA was isolated from tissues with TRIzol (Invitrogen). RNA was used to generate cDNA using the MLV-V reverse transcriptase with random primers (Invitrogen). RT-PCR was performed on the Strategene MX3005. Data were normalized to two housekeeping genes (*Ppia* and *36B4*) based on Genorm algorithm (medgen.ugent.be/genorm/) and expressed as fold changes relative to control tissues. Supplementary Table S2 lists the RT-PCR primer sequences for genes that were analyzed.

2.8. Immunoblot analysis

Tissues were homogenized and lysed in lysis buffer as previously described [40]. The protein concentration was determined by Bradford protein assay (Bio-Rad). Equal amounts of proteins were loaded and immunoblot analyses were carried out according to standard protocol. The following antibodies from Cell Signaling Technologies were used: HSL (4107), Phospho-HSL (Ser563) (4139), ATGL (2138), HSP60 (12165), DRP1 (5391), phosphor-DRP1 Ser616 (4494), phosphor-DRP1 Ser637 (4867), phosphor-AKT Ser473 (4060), AKT (9272), and LC3A/B (4108). Total OXPHOS Rodent WB Antibody Cocktail (ab110413), MLKL (ab172868), Anti-RIP3 (phosphor T231 + S232) (ab201912), and UCP1 (ab1426) were obtained from Abcam. GAPDH (60004-1-IG) and P62 (18420-1-AP) were obtained from Proteintech; PLIN1 (GP29, Progen Biotechnik GmbH); β-actin (MAB1501, MilliporeSigma); RIPK3 (NBP1-77299SS, Novus Biologicals).

2.9. Statistical analysis

Quantitative data were presented as means ± SEM. Differences between groups were examined for statistical significance with either unpaired t test corrected for multiple comparisons using the Holm–Sidak method, or two-way ANOVA followed by Tukey's post-hoc tests using Prism 8 software. A *P* value of less than 0.05 was considered statistically significant.

3. RESULTS

3.1. Deletion of BSCL2 in mature brown adipocytes induces SNS-independent cAMP/PKA signaling and reduces BAT and circulating triglyceride levels at thermoneutrality

Previously, we have demonstrated that deletion of *Bscl2* in Myf5+ progenitors does not affect brown adipogenesis but activates SNS-independent cAMP/PKA signaling to enhance lipid oxidation and uncoupling in BAT, leading to atrophy of the BAT depot [42]. To examine the in vivo function of BSCL2 in a more BAT-specific manner, we generated a mouse model lacking BSCL2 in mature brown adipocytes. $Bscl2^{UCP1\text{-}BKO}$ (BKO) mice were obtained by breeding $Bscl2^{f/f}$ mice with transgenic mice expressing UCP1 promoter driven Cre recombinase, which is only active in mature brown adipocytes [47]. The littermate Cre negative $Bscl2^{f/f}$ mice were used as a wild-type control (Ctrl). We found the *Bscl2* expression was deleted by >90% in BAT but not epididymal WAT (eWAT) and subcutaneous WAT (sWAT) of BKO mice (Figure 1A). We were not able to confirm the deletion of BSCL2 at the protein level due to the lack of a specific antibody to detect endogenous murine BSCL2. To examine whether the deletion of BSCL2 in mature brown adipocytes also elicits SNS-independent cAMP/PKA signaling, we first housed BKO mice from weaning for 12 weeks in a thermoneutral environment (30 °C), in which sympathetic activity is minimal. Indeed, BKO BAT displayed enhanced cAMP/PKA-mediated HSL phosphorylation without changing HSL and ATGL expression (Figure 1B). The mRNA expression of BAT-specific marker genes such as *Pgc1α, Ucp1, Dio2* and *Cox8b* were comparable between the two genotypes (Figure 1C). Although body weights of the two genotypes were similar (Ctrl: 27.76 ± 0.58 vs BKO: 27.64 ± 0.45), BAT masses in BKO mice trended lower (Figure 1D). Histological analyses revealed fewer and smaller lipid droplets (LDs) in BAT of BKO mice, compared with more WAT-like LDs in BAT of control mice housed in a warm environment (Figure 1E). Total TG content per BAT depot was significantly decreased in BKO mice (Figure 1F), consistent with increased cAMP/PKA-mediated TG hydrolysis. Total nuclear DNA (nDNA) content per BAT depot was similar for the two genotypes, suggesting a maintained brown adipocyte number (Figure 1G). Interestingly, activation of cAMP/PKA signaling in BAT of BKO mice housed at thermoneutrality showed reduced circulating levels of TG (Figure 1H), but not NEFA (Figure 1I) or glucose (Figure 1J). Percent body fat (Figure 1K), and eWAT and sWAT masses (Figure 1L) were not changed in BKO mice. These data confirm a cell-autonomous role for BSCL2 in mediating cAMP/PKA signaling in mature brown adipocytes independent of SNS activity, and imply that deletion of BSCL2 activates a presumably quiescent BAT sufficiently to reduce circulating TG in mice protected from thermal stress.

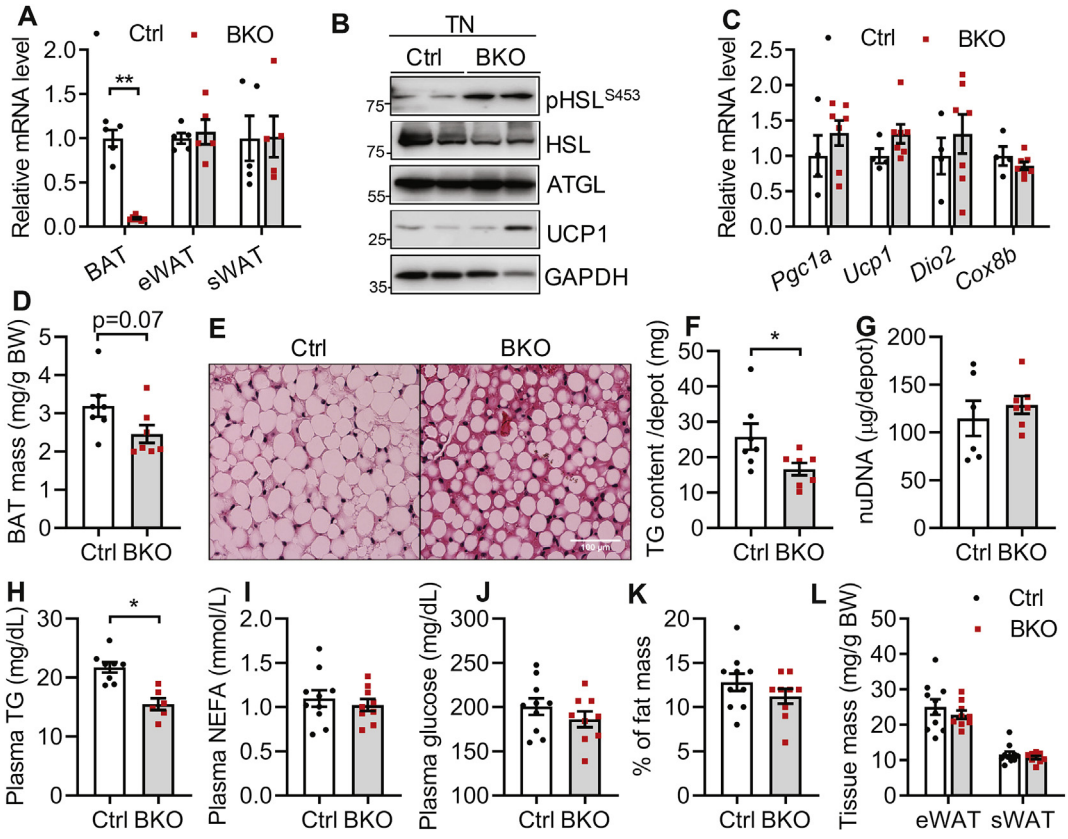

Figure 1: BSCL2 deletion in mature brown adipocytes activates brown adipose tissue and reduces plasma triglycerides at thermonutrality. (A) mRNA analysis of brown adipose tissue (BAT), epididymal (eWAT) and subcutaneous white adipose tissue (sWAT) in 10 weeks old male Ctrl and *Bscl2*$^{UCP1\text{-}BKO}$ (BKO) mice housed at room temperature of 21 °C. (B) Immunoblots of cAMP/PKA signaling and UCP1 in BAT; (C) qPCR analysis of BAT marker genes; (D) BAT mass as normalized to body weight (BW); (E) H&E staining of BAT; (F) total triglyceride (TG) contents in whole BAT depots; (G) total nuclear DNA (nDNA) contents in whole BAT depots; (H) plasma TG; (I) plasma NEFA; (J) plasma glucose; (K) % of fat mass; and (L) eWAT and sWAT masses as normalized to BW in male Ctrl and BKO mice housed at 30 °C for 12 weeks since weaning. $*P < 0.05$; $**P < 0.005$ vs Ctrl mice. N = 6–10/group.

3.2. BSCL2 deletion in brown adipocytes reduces BAT TG and mass but does not affect whole-body metabolic homeostasis under ambient temperature

We next examined BAT and metabolic phenotype of BKO mice housed at 21 °C (RT), which confers a mild thermal stress. When housed at RT, control and BKO mice maintained similar body weights (Fig. S1A) and whole-body adiposity (Fig. S1B) at both 3 months (M) and 9 months of age. RT housing caused a ~30% reduction of BAT mass in 3 months old BKO mice (Figure 2A) and a ~70% reduction as mice aged to 9 months (Fig. S1C). Histological analyses revealed a severe loss of multi-lobular LDs accompanied by the appearance of occasional supersized unilobular LDs in BAT of 3 months old BKO mice housed at RT (Figure 2B). Total TG content of the whole BAT depot of BKO mice was reduced by ~40% as compared to control mice housed at RT (Figure 2C). BKO BAT retained an increased cAMP/PKA-mediated HSL phosphorylation without perturbing HSL or ATGL expression (Figure 2D), suggesting that activation of cAMP/PKA signaling reduced TG content in BSCL2-deleted BAT. Despite reductions in BAT mass and TG content, 3 months old BKO mice displayed no change in food intake, VO2 consumption, heat production, respiratory exchange ratio (RER) or physical activity (Figs. S1D–H, respectively). Glucose clearance and insulin sensitivity were also similar in control and BKO mice (Figs. S1I–J). Specifically, we found no differences in the basal and insulin-stimulated AKT phosphorylation at Ser473 in BAT of control and BKO mice (Fig. S1K); suggesting BSCL2 deletion in BAT did not autonomously alter its insulin signaling. These data demonstrate that BSCL2 deletion in mature brown adipocytes activates cAMP/PKA signaling, reduces BAT TG contents and mass, but does not change whole-body metabolism in BKO mice housed at RT.

3.3. BSCL2 deletion in mature brown adipocytes leads to cold intolerance associated with defective thermogenic programing

To test whether reduced BAT TG and mass in BKO mice influenced adaptive thermogenesis, we exposed ad libitum-fed, 3 months old BKO mice to an ambient temperature of 4 °C. We found no change in rectal temperature between two genotypes housed at RT (0 h in Figure 2E), but chronic cold exposure (CE) at 4 °C led to the development of hypothermia within 72 h in BKO, but not control mice (Figure 2E). BKO mice also became rapidly hypothermic when exposed to 4 °C in the absence of food (Fig. S1L). Cold intolerance was exaggerated in ad libitum-fed 9 months old BKO mice, which developed hypothermia within only 12 h, consistent with the atrophy of BAT in these animals (Fig. S1M). These data indicate that the loss of BSCL2 in mature brown adipocytes impairs non-shivering thermogenesis.

We then examined whether impaired thermogenesis in BKO mice is due to defective lipolysis in WAT, which supplies NEFA critical for thermogenesis [15]. While plasma TG and NEFA levels were similar between the two genotypes housed at RT, hypothermia in cold-

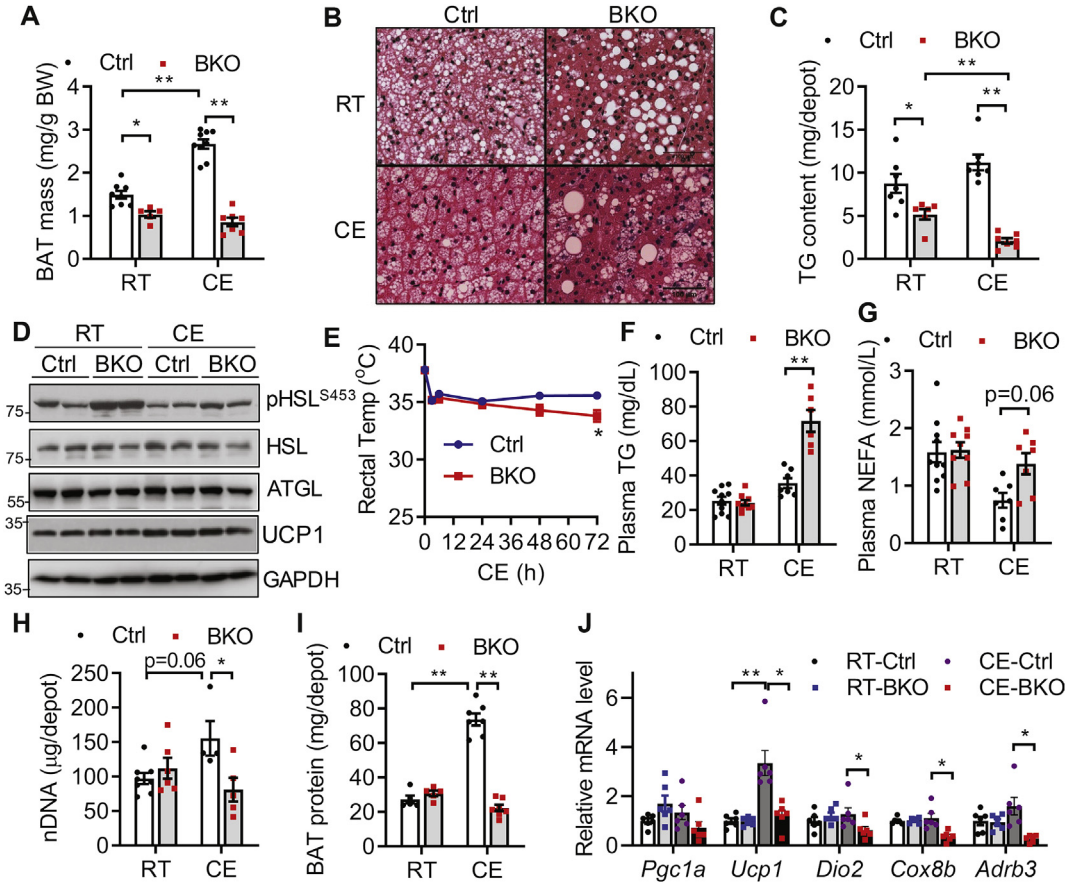

Figure 2: *Bscl2*$^{UCP1\text{-}BKO}$ mice fail to recruit brown adipose tissue and maintain thermogenesis under cold acclimation. (A) BAT masses as normalized to body weight (BW); (B) H&E staining of BAT; (C) total triglyceride (TG) contents in whole BAT depots; (D) immunoblots of marker proteins for lipolysis in 3 months (M) old Ctrl and *Bscl2*$^{UCP1\text{-}BKO}$ (BKO) mice housed at room temperature (RT) of 21 °C and after 3 days of cold exposure (CE) at 4 °C. (E) Rectal core body temperature of 3M old Ctrl and BKO male mice during 3 days of CE in the presence of food, n = 10/group. (F) Plasma TG; (G) plasma NEFA; (H—I) total nuclear DNA (nDNA) (H) and protein (I) contents in whole BAT depots; (J) relative mRNA expression of classical brown fat genes in 3M old Ctrl and BKO male mice housed at RT and after 3 days of CE. N = 6—10/group. $^{*}P < 0.05$; $^{**}P < 0.005$.

exposed, ad libitum-fed BKO mice was associated with significantly elevated circulating levels of TG (Figure 2F) and NEFA (Figure 2G). There were no differences in the mass of either eWAT or sWAT in the two genotypes housed at RT (Figs. S2A—B), consistent with their similar adiposity (Fig. S1B). Chronic CE led to an equivalent reduction in WAT mass for both genotypes (Figs. S2A—B). Histology showed normal subcellular structures in both eWAT and sWAT in both genotypes housed at either RT or 4 °C (Fig. S2C). Reduced BAT mass in BKO mice did not cause WAT browning, as the expression of beige adipocyte marker genes in sWAT of BKO mice was similar to that in control mice housed at RT, and even trended lower during CE (Fig. S2D). Together, these data suggest that BKO mice develop cold intolerance due to BAT dysfunction and a failure to induce WAT browning, rather than abnormal WAT lipolysis.

Cold acclimation induces BAT recruitment to maintain long-term cold tolerance. In chronic cold-exposed control mice, BAT mass (Figure 2A), the total BAT nDNA (Figure 2H) and protein (Figure 2I) per BAT depot were significantly elevated as compared to RT-housed control mice, suggesting BAT recruitment. However, BAT thermogenic reprograming was blunted in BKO mice, as BAT mass (Figure 2A); nDNA (Figure 2H) and protein (Figure 2I) contents in BKO BAT failed to rise and were even markedly reduced as compared to cold-acclimated control mice. In addition, CE induced the expected accumulation of more multi-lobular small LDs in control BAT (Figure 2B). However, it further exaggerated loss of LDs from BKO BAT, with the appearance of only a few typical multi-lobular brown adipocytes and more leukocytes infiltration (Figure 2B). TG content in BAT of BKO mice was further depleted to only 18% of that in control mice after chronic cold exposure (Figure 2C). Comparison of BAT marker gene expression found no differences between the two genotypes housed at RT. In response to CE, the mRNA expression of *Ucp1* increased 3.5 fold in BAT of control mice (Figure 2J), so was its protein level (Figure 2D), confirming BAT recruitment. However, CE significantly downregulated the mRNA expression of the thermogenic genes *Ucp1*, *Dio2, Cox8b* and *Adrb3* (Figure 2J) in BKO BAT, though its reduction of UCP1 at protein level was not obvious (Figure 2D). Collectively, our data suggest that BSCL2-deleted BAT fails to elicit thermogenic reprograming and undergoes remarkable brown adipocyte loss in response to physiological cold stimulation.

3.4. BSCL2 deletion in brown adipocytes is associated with inflammation, macrophage infiltration and fibrosis in brown adipose tissue

To identify the link between BSCL2 deletion and altered BAT function in BKO mice, we performed an unbiased RNA-seq analysis of BAT isolated from control and BKO mice housed at RT. Among 12,966 genes

surveyed, only 99 were differentially expressed ($1.0 \leq Log_2FC \leq -1.0$; adj. $P < 0.05$). Of these, 84 were upregulated and 15 were downregulated (Supplemental Table S1). No significant transcriptional changes in genes involved in de novo lipogenesis, TG synthesis, or lipolysis were identified, suggesting a major post-transcriptional regulation of lipid metabolism in BKO BAT (GEO accession#: GSE145070). Intriguingly, GO analysis based on biological function identified two major functional pathways that were significantly altered: regulation of immune response (GO:00507676) and leukocyte activation (GO:0045321). A gene signature related to leukocyte activation was particularly interesting, as it is known to regulate adipose tissue inflammation and remodeling (Figure 3A). Indeed, macrophage marker genes such as *Emr1* (a.k.a. *F4/80*), *Lgals3* (a.k.a. *Mac2*), the M1 macrophage marker *Cd68*, and *Mmp12*, a relative macrophage specific metalloelastase shown to be activated by lipolytic remodeling [48], were among those that were highly upregulated in RT-housed BKO BAT. RT-PCR confirmed the upregulation of these macrophage marker genes in BAT of BKO mice at RT (Figure 3B). This upregulation was more robust in BKO BAT after chronic CE (Figure 3B). Interestingly, the M2 macrophage marker gene (*Mrc1*) was also elevated in cold-acclimated BKO BAT, suggesting the recruitment of both M1 and M2 macrophages after thermogenic insult (Figure 3B). However, the recruitment of macrophages was not associated with significant increases in the mRNA levels of proinflammatory cytokines, such as *Tnfα*, *Ccl2* and *IL1β*, in BKO BAT housed at either RT or 4 °C (Figure 3C). We next performed Galectin 3 staining to confirm macrophage infiltration into BAT. There was a slightly more immunoreactive staining of Galectin 3 (brown color) in BAT of BKO mice housed at RT. Consistent with its mRNA expression, Galectin 3-positive staining was dramatically elevated in BAT of chronically cold-exposed BKO mice (Figure 3D). Adipose tissue inflammation is normally associated with fibrosis. We found genes

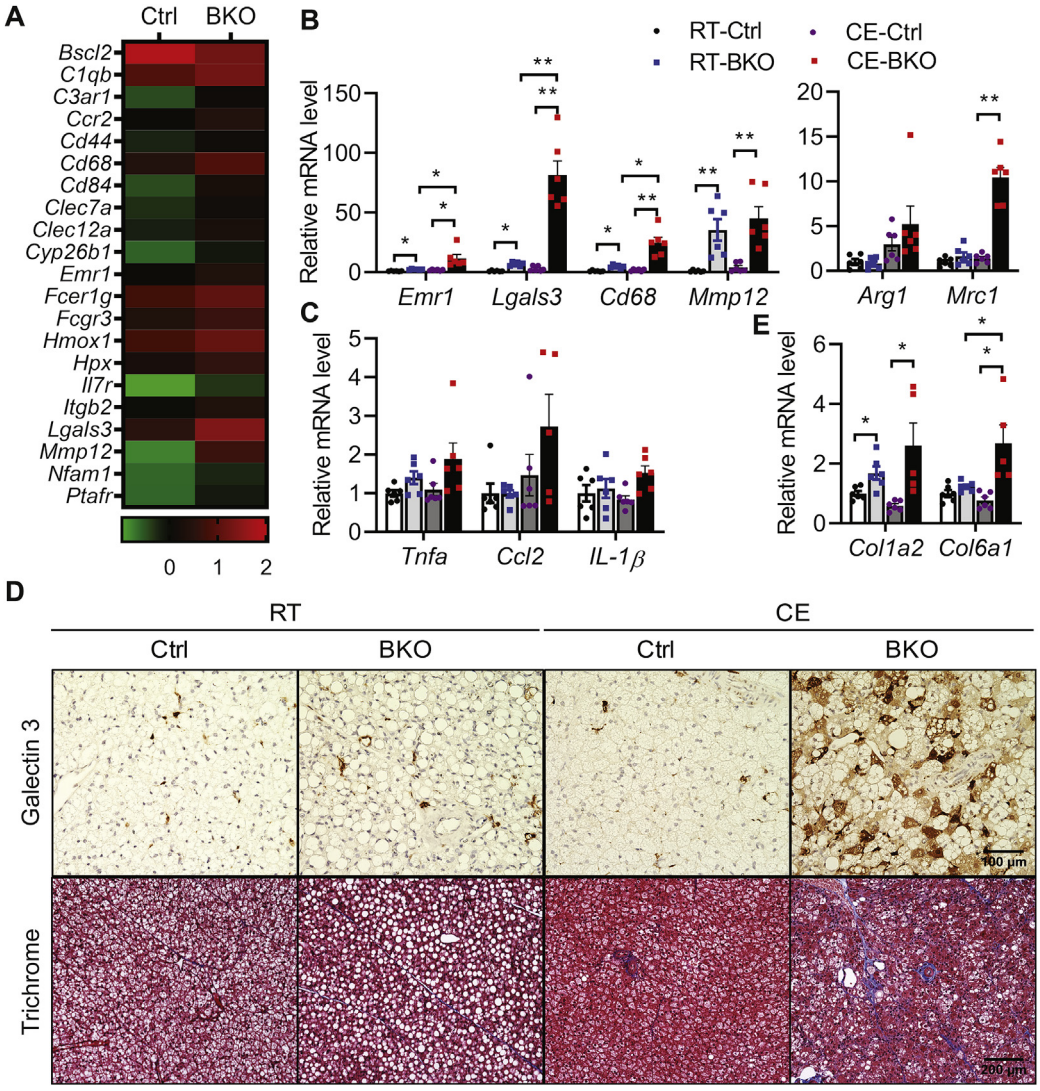

Figure 3: BSCL2 deletion in brown adipocytes induces brown adipose tissue macrophage infiltration, inflammation and fibrosis. (A) Heatmap of inflammation related differentially expressed genes (DEGs, $1.0 \leq Log_2FC \leq -1.0$; adj. $P < 0.05$) identified from RNA-seq analysis of 10 weeks old male Ctrl and *Bscl2*$^{UCP1\text{-}BKO}$ (BKO) BAT (n = 3 with each pooled from 3 animals) housed at room temperature (RT) of 21 °C. Relative expression values (Z-scaled log2 [TPM]) for the 21 genes are illustrated, including macrophage marker genes, cytokine or cytokine receptor or inflammatory mediators, and *Bscl2* gene. A summary table of DEGs is presented in Table S1. (B–C) RT-PCR of marker genes for macrophages (B) and proinflammatory cytokines (C); (D) Galectin 3 immunohistochemistry and trichrome staining of BAT; and (E) RT-PCR of marker genes for fibrosis in BAT of 3 months old Ctrl and BKO male mice housed at RT and after 3 days of cold exposure (CE) at 4°. $P < 0.05$; $^{**}P < 0.005$. N = 6–10/group.

involved in adipose tissue fibrosis (*Col1a2*, and *Col6a1*) were minimally upregulated in BAT of BKO mice housed at RT, but more robustly elevated after CE (Figure 3E). Trichrome staining further confirmed increased fibrosis, especially in BAT of BKO mice after cold acclimation (Figure 3D). These data suggest that BSCL2 deletion in mature brown adipocytes causes significant BAT pathological remodeling potentiated by thermogenic stress.

3.5. BSCL2 deletion in mature brown adipocytes increases mitochondrial uncoupling in vitro but causes mitochondrial dysfunction in vivo

Cold induced-cAMP/PKA signaling stimulates brown adipocyte mitochondrial uncoupling and fission [49]. We next examined whether BSCL2-mediated cAMP/PKA signaling also regulates BAT mitochondrial bioenergetics and dynamics. We first performed respiration analysis of isolated mitochondria from BAT of control and BKO mice housed at RT. Not surprisingly, isolated BKO mitochondria exhibited higher basal and maximal OCR. The elevated basal mitochondrial OCR was largely attributable to increased uncoupling with only a tendency for lower coupled OCR (Figure 4A, B). Elevated uncoupling in BAT mitochondria of BKO mice was not due to differences in UCP1 protein abundance (Figure 4C). BSCL2 deletion did not affect the levels of marker proteins for each of the electron transport chain (ETC) complexes expressed per μg mitochondrial protein (Figure 4C). These data suggest that BSCL2 deletion in brown adipocytes is coupled to mitochondrial hyperactivity, emphasizing an important cell-autonomous role of BSCL2 in regulating mitochondrial uncoupling.

To examine BSCl2-mediated mitochondrial function in a more physiological relevant setting, we performed TEM of BAT from control and BKO mice housed at RT. TEM first confirmed largely reduced numbers of LDs with either minute or supersized LD sizes present in the brown adipocytes of BKO mice (Figure 4E1) compared with those in control mice (Figure 4D1). The mitochondrial ultrastructure in BAT of Ctrl mice was intact with dense and well-organized cristae (Figure 4D2). Surprisingly, the cytoplasm of almost every single BKO brown fat cell was densely packed with mitochondria (Figure 4E1—F1). These cells were heterogeneous, as they contained at least three types of mitochondrial ultrastructural shapes, including sphere mitochondria with intact cristae ('M' in Figure 4E2), sphere mitochondria with severely disorganized cristae (* in Figure 4E2) and elongated tubular mitochondria with dense cristae (arrow in Figure 4E2 and G). Interestingly, the dominant fission phenotype in BKO BAT was associated with neither changes in the expression of mitochondrial pro-fission protein DRP1 nor PKA-mediated DRP1 phosphorylation in the equivalent serine

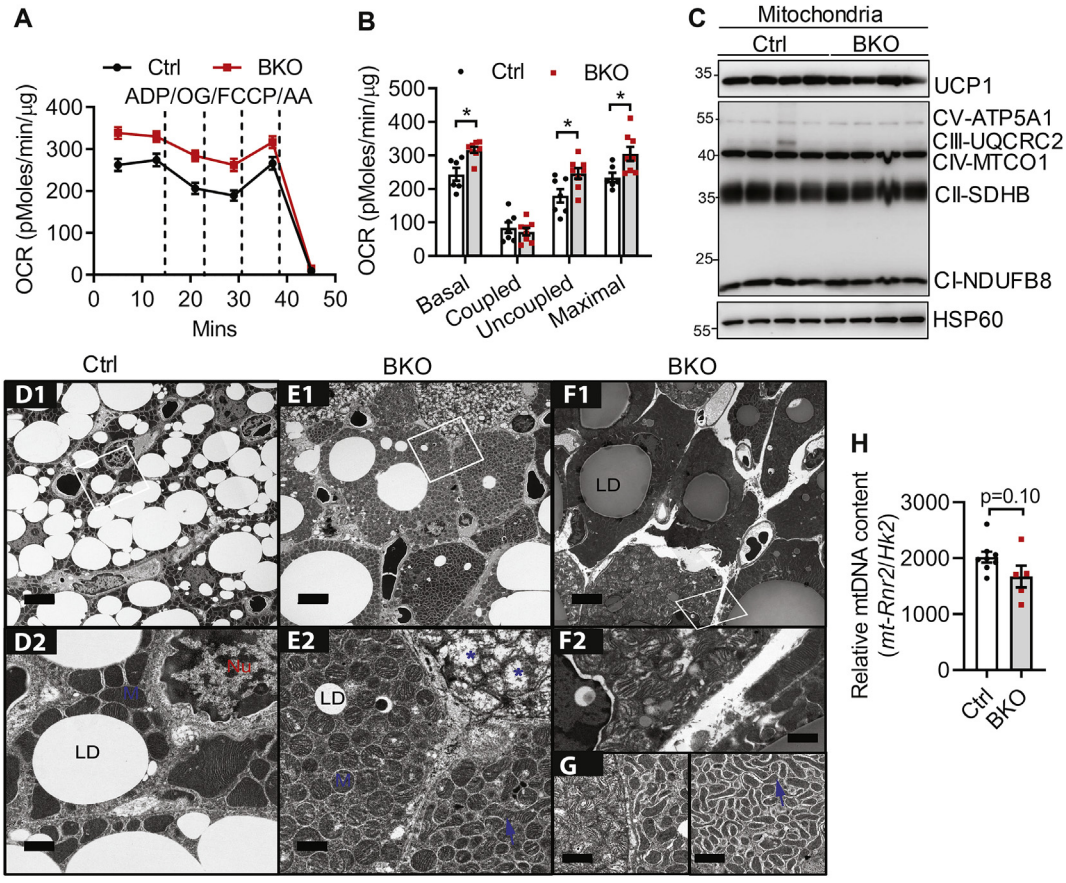

Figure 4: BSCL2 regulates mitochondrial activity and dynamics in brown adipose tissue. (A—B) The coupling assays were performed in isolated BAT mitochondria to assess oxygen consumption rates (OCR) with sequential addition of ADP, oligomycin (OG), FCCP and antimycin A (AA). Basal, coupled, uncoupled and maximal mitochondrial respiration were shown in (B). 3 months old male mice housed at room temperature (RT) of 21 °C were used, n = 7—8 in triplicates. (C) Immunoblots of isolated mitochondria, n = 4/group. (D—G) Representative transmission electron micrographs of BAT from 3M old Ctrl and BKO mice housed at RT. D1, E1, F1: scale bars = 5 μm; D2, E2, F2 and G: scale bars = 1 μm. Lipid droplet (LD), nucleus (Nu), mitochondria (M). Blue arrows point to the elongated mitochondria; blue asterisks indicate dysmorphic mitochondria. N = 3/group. (H) Relative mtDNA content in BAT assessed by RT-PCR and calculated from copy numbers of the mtDNA-encoded *mt-Rnr2* gene and the nuclear DNA-encoded *Hk2* intron 9 gene (N = 5—7/group). $*P < 0.05$; $**P < 0.005$ vs Ctrl mice.

to humane Ser637 (Fig. S3). We also found no differences in the cyclin-dependent kinase (CDK)-mediated DRP1 phosphorylation in the equivalent serine to human Ser616 (Fig. S3). Some BSCL2-deleted brown adipocytes were completely devoid of LDs and were tiny with reduced numbers of mitochondria (Figure 4E1—F1). As such, there was a tendency for a lower ratio of mtDNA-encoded *MT-Rnr2* to nDNA-encoded *Hk2* intron 9 in BKO BAT (Figure 4H). The prevalence of brown adipocytes containing fragmented mitochondria with disrupted cristae in BKO mice indicates that BSCL2 deletion in BAT increases mitochondrial dysfunction and the loss of mitochondrial DNA. Collectively, these data suggest that BSCL2 deletion-induced cAMP/PKA signaling in mature brown adipocytes is intrinsically linked to progressive mitochondrial dysfunction in vivo.

3.6. BSCL2 deletion in brown adipocytes is associated with mitochondrial DNA depletion and necroptosis after chronic cold acclimation

Chronic cold exposure caused a severe loss of brown adipocyte numbers in BKO BAT (Figure 2), but the pathway responsible for this has not been identified. TUNEL staining and western blotting of cleaved caspase 3 and PARP1 (data not shown) failed to identify apoptotic cells. Receptor-interacting serine—threonine kinases 3 (RIPK3) and mixed-lineage kinase domain-like protein (MLKL) are key mediators of necroptosis, a programmed necrotic cell death pathway [50,51]. Interestingly, while there were no differences in the expression of these proteins in BAT of mice housed at RT, chronic CE led to a strong induction of MLKL and RIPK3 expression in BAT of BKO mice (Figure 5A, B). A similar increase was observed in RIPK3 phosphorylation (Figure 5A, B), which corresponds to its kinase activity [50]. These data suggest that BSCL2-deleted brown adipocytes undergo necroptosis during chronic cold stress.

Necroptosis is associated with depolarized mitochondria and ATP depletion [52]. We found that chronic cold acclimation decreased the mtDNA number in the residual BKO BAT, confirming defects in mitochondrial biogenesis after cold acclimation (Figure 5C). TEM of BAT demonstrated depletion of LDs in most residual BKO brown adipocytes (Figure 5E1) in contrast to the accumulation of multi-lobular LDs in control brown adipocytes (Figure 5D1). Mitochondrial dropout was frequently observed, accompanied with basal membrane rupture and the presence of necrotic cells in BKO BAT (Figure 5E2—F2). Specifically, we detected severely fragmented cellular remnants in the extracellular space and in neighboring macrophages in BKO BAT, suggesting that those remnants were being engulfed by macrophages (Figure 5G1, G2). Collectively, our biochemical and ultrastructural data

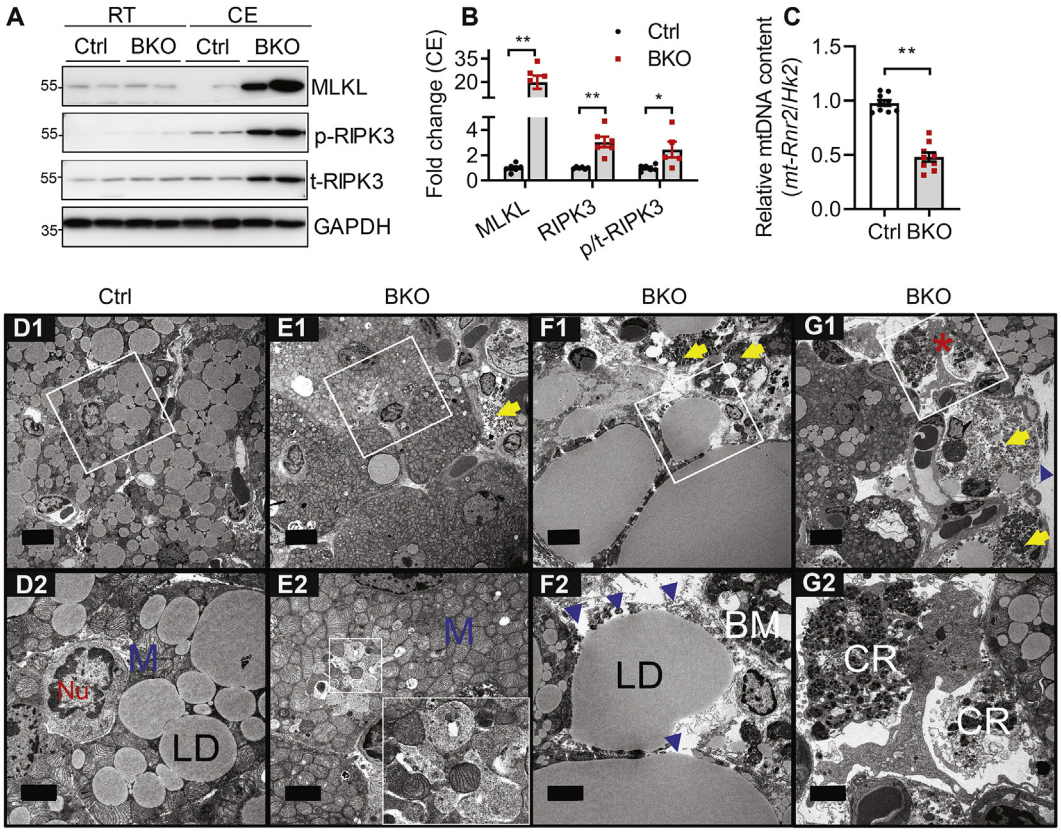

Figure 5: *Bscl2*$^{UCP1\text{-}BKO}$ brown adipose tissue undergoes necroptosis in response to chronic cold stress. (A) Western blotting of necroptotic marker proteins in BAT of 3 months (M) old Ctrl and *Bscl2*$^{UCP1\text{-}BKO}$ (BKO) male mice housed at room temperature (RT) of 21 °C and after 3 days of cold exposure (CE) at 4 °C. p-RIPK3: phosphorylated RIPK3; t-RIPK3: total RIPK3. (B) Quantification of protein levels in BAT of Ctrl and BKO mice housed for 3 days of CE. Data were normalized to Ctrl after CE. N = 5—6/group. (C) Relative mtDNA content in BAT assessed by RT-PCR and calculated from copy numbers of the mtDNA-encoded *mt-Rnr2* gene and the nuclear DNA-encoded *Hk2* intron 9 gene (n = 9—10/group). (D—G) Representative transmission electron micrographs of BAT from 3M old Ctrl and BKO mice after 3 days of CE at 4 °C. Scale bar = 5 μm for D1, E1, F1, G1. Inserts were shown in D2, E2, F2, G2 respectively with scale bar = 2 μm. Lipid droplet (LD), nucleus (Nu), mitochondria (M). Note the donut shape mitochondria and mitochondrial dropouts in E2 which was further enlarged in white square, (8000×). Evidence of necroptosis includes disrupted basal membrane (BM) (blue arrowheads) and cytoplasmic remnants (CR). Yellow arrows indicate late necroptotic cells. Red asterisk in G1 indicates cytoplasmic remnants being engulfed by a macrophage which was further enlarged in G2. N = 3/group. $^{*}P < 0.05$; $^{**}P < 0.005$.

demonstrate for the first time that BSCL2 deletion in mature brown adipocytes ultimately causes mitochondrial depletion and necroptosis of brown adipocytes under chronic cold stress.

3.7. Chronic CL 316,243 injection exacerbates brown adipocyte necroptosis, inflammation and macrophage infiltration in mice with brown adipocyte-specific deletion of BSCL2

The selective β3-adrenoceptor agonist CL is commonly used to mimic a cold-challenge [1]. To understand the role of BSCL2-mediated lipid catabolism on the physiology of thermogenic plasticity, we treated control and BKO mice with CL or PBS for 5 days. Gross examination revealed that CL injection did not alter the BAT mass of control mice but reduced that of BKO mice (Figure 6A). This was confirmed by marked suppression of mRNA expression of BAT marker genes in BAT of CL-injected BKO mice (Figure 6B). UCP1 protein level was also significantly downregulated in BAT of CL-injected BKO mice (Figure 6C). The protein levels of MLKL, RIPK3 phosphorylation and total RIPK3 were dramatically increased in CL-injected BKO BAT, indicating that necroptosis of brown adipocytes was induced by CL treatment (Figure 6C). Histological examination revealed a depletion of multi-lobular LDs in BAT of BKO mice; in contrast to the accumulation of smaller LDs in BAT of control mice (Figure 6D). When examining BAT for markers of macrophage infiltration, we found increased expression of macrophage marker genes such as *Emr1* and *Lgals3* in BAT of PBS-injected BKO mice, which was further upregulated after CL injection (Figure 6E). Galectin 3 staining confirmed increased macrophage infiltration of BAT from CL-injected BKO mice, consistent with a greater infiltration of inflammatory immune cells (Figure 6D). CL injection also exacerbated BAT fibrosis, illustrated by increased mRNA expression of collagen genes (*Col1a2* and *Col6a1*) (Figure 6F) and by trichrome staining (Figure 6D). Together, these data highlight a failure of reprograming in BSCL2-deleted BAT in response to a pharmacological stimulation of thermogenesis.

3.8. Deletion of BSCL2 in mature brown adipocytes is protective against circulating hypertriglyceridemia but not diet-induced obesity

Finally, we tested whether BSCL2-mediated brown adipocyte function plays a role in diet-induced obesity. When mice were fed an HFD for up to 18 weeks at RT, we found no differences in body weights (Figure 7A) or whole body adiposity (Figure 7B) between the two genotypes. There was a 55% reduction in BAT mass of HFD-fed BKO mice compared to control mice (Figure 7C). Histology revealed the whitening of control BAT characterized by increased numbers and sizes of LDs. These changes were not apparent in BAT from HFD-fed BKO mice, which contained much fewer LDs (Figure 7D). The total TG content per BAT depot in BKO mice was 60% less than that in control mice (Figure 7E). However, HFD also induced brown adipocyte loss in BKO mice, as evidenced by a 10% reduction in total nDNA content (Figure 7F). Even though UCP1 expression was comparable between the two genotypes, there was a slight upregulation of MLKL and phosphorylation of RIPK3, indicating the presence of necroptosis (Figure 7G). Similar to BKO mice housed at thermoneutrality, we found a reduced serum TG level in BKO

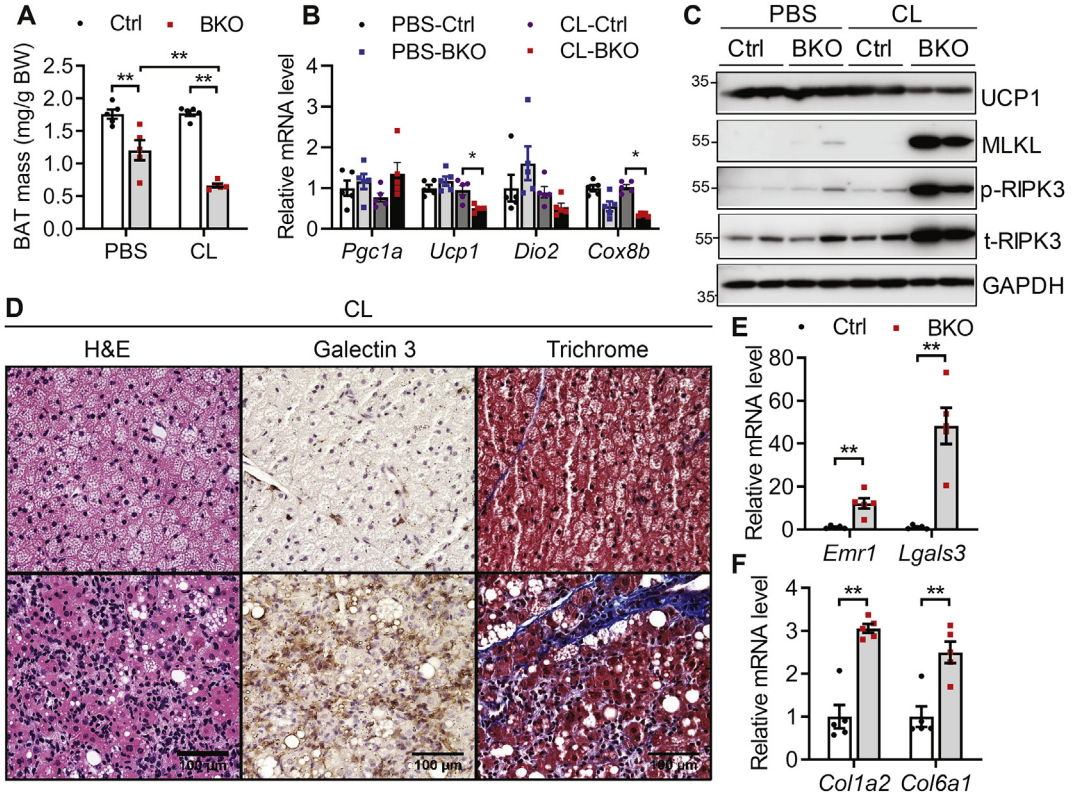

Figure 6: Chronic adrenergic activation accelerates brown adipose tissue necroptosis, inflammation and fibrosis. (A) BAT mass as normalized to body weight (BW); (B) relative mRNA expression of classical brown fat genes; (C) representative immunoblots of marker proteins for BAT and necroptosis (p-RIPK3: phosphorylated RIPK3; t-RIPK3: total RIPK3); (D) H&E staining, Galectin 3 immunohistochemistry and trichrome staining of BAT; (E–F) qPCR of marker genes for inflammation and fibrosis. A, B, C, E and F were performed in BAT of 3 months old male Ctrl and *Bscl2*$^{UCP1\text{-}BKO}$ (BKO) mice after 5 days of PBS or CL 316,243 (CL) injection. D was performed in CL-injected BAT. $^{*}P < 0.05$; $^{**}P < 0.005$. N = 5/group.

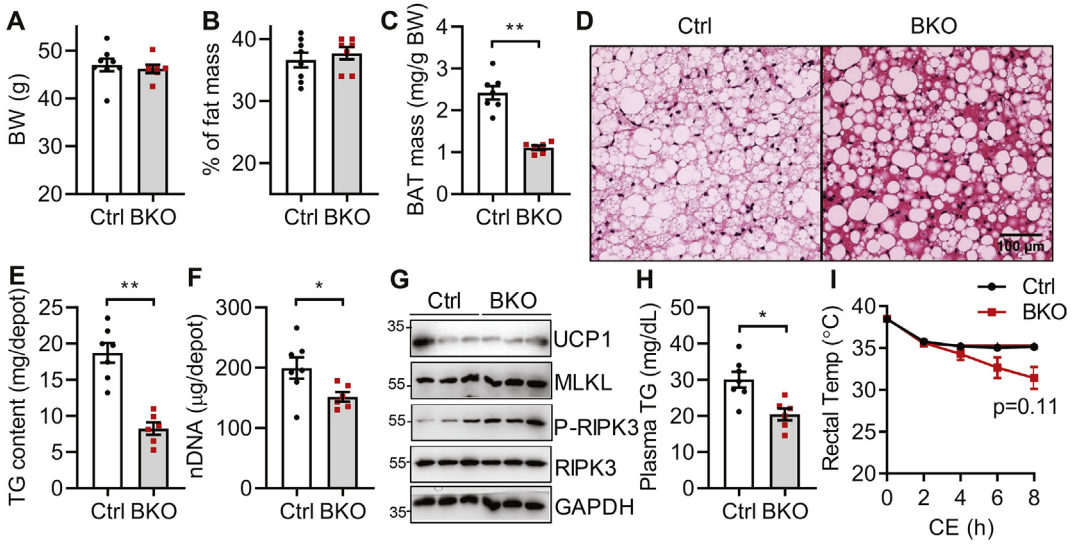

Figure 7: Deletion of BSCL2 in mature brown adipocytes reduces circulating triglycerides but not obesity in *Bscl2*$^{UCP1\text{-}BKO}$ mice fed with high fat diet. (A) Body weight (BW); (B) % of fat mass; (C) BAT mass as normalized to BW; (D) H&E-stained BAT; (E) total triglyceride (TG) contents in whole BAT depots; (F) total nuclear DNA (nDNA) contents in whole BAT depots; (G) immunoblots of BAT marker and necroptosis proteins; (H) plasma TG and (I) rectal body temperature upon acute cold exposure (CE) at 4 °C under fasting. Male Ctrl and BKO mice fed with 60% high fat diet for 18 weeks since weaning were used. $^{**}P < 0.005$ vs Ctrl mice. N = 6–10/group.

mice as compared to control mice fed HFD, suggesting that the remaining BSCL2-deleted BAT was utilizing more circulating lipids (Figure 7H). HFD feeding improved the cold tolerance of BKO mice, which started to develop hypothermia after 8 h of cold exposure in the absence of food (Figure 7I). These data suggest that enhanced BAT energetics, even with a reduced BAT mass, can improve the circulating lipid profile but fails to alleviate diet-induced obesity.

4. DISCUSSION

Using a mouse model with BSCL2 specifically deleted in mature brown adipocytes, the present study identifies for the first time a cell-autonomous role of BSCL2 in regulating mature brown adipose mass/activity and thermogenic function. BSCL2 deletion in mature brown adipocytes is associated with enhanced cAMP/PKA-mediated lipolysis in a SNS-independent manner, which results in a temperature and age-dependent loss of BAT lipids and masses and ultimately leads to severe cold intolerance in *Bscl2*$^{Ucp1\text{-}BKO}$ mice. We further demonstrate that BSCL2 deletion in mature brown adipocytes stimulates lipid catabolism which uncouples brown adipocytes and induces necroptosis in response to a thermogenic challenge. These novel findings suggest that BSCL2 control of lipid metabolism is essential for BAT cellular and tissue maintenance.

BAT thermogenic potential is inversely correlated with body weight and susceptibility to obesity across many mouse models [53]. However, BSCL2 deletion-induced BAT activation through cAMP/PKA signaling was only able to minimally ameliorate plasma TG levels under thermoneutral and high fat diet conditions but had little effect on the progression of obesity regardless of ambient temperature or diet. In contrast, *Bscl2*$^{Ad\text{-}mKO}$ mice, in which BSCL2 is deleted in both mature white and brown adipose tissue, are much leaner and protected from diet-induced obesity, especially when housed under thermoneutrality [40]. This suggests that BSCL2 deletion-induced activation of brown adipose bioenergetics alone is not sufficient for the homeostatic regulation of obesity. Meanwhile, our *Bscl2*$^{UCP1\text{-}BKO}$ mice displayed complete cold sensitivity with maintained adiposity, which is in sharp contrast to both *Bscl2*$^{Ad\text{-}mKO}$ and *Bscl2*$^{Myf5\text{-}BKO}$ mice. Deletion of BSCL2 in Myf5+ precursor cells results in a more severe BAT atrophy but ultimately higher white adiposity and unaltered BAT thermogenic response to cold acclimation [42]. These differences between genotypes could be attributed to the different developmental stages of BSCL2 deletion in BAT and the presence of Myf5+ cells in depots other than BAT [54]. Taken together, these unique animal models highlight the complexity of BAT physiology and the importance of WAT/BAT cross-talk in mediating adaptive thermogenesis.

It seems logical that enhancing the ability to burn lipid stores within brown adipocytes could render mice resistant to cold. Therefore it is somewhat counterintuitive that BKO mice are completely cold intolerant under acute or chronic cold exposure (Figure 2). Lipid stores in BAT may be essential for an appropriate response to a thermal stress which has been previously reported in the SOD2KO model [55]. Meanwhile, the deletion of BSCL2 in mature brown adipocytes causes a relentless catabolism of BAT lipid, which may be sufficient to uncouple brown fat mitochondria to the point that the cells die under chronic cold exposure. A similar phenomenon is reported from Ap2-UCP1 homozygous transgenic mice, in which excessive expression of UCP1 from the transgene results in a collapse of energy metabolism, leading to BAT atrophy and cold intolerance [56]. In our BKO mice, long-term thermogenic activation triggered by cold exposure or CL injection completely failed to activate BAT recruitment. Instead, it accelerated brown adipocyte death. Therefore activation of these thermogenic pathways was not merely refractory in BKO mice but was detrimental. The cold intolerance of BKO mice was not due to a lack of circulating substrate availability, as their serum levels of TG and NEFA were significantly elevated during cold exposure (Figure 2F, G). These data support the notion that intracellular multi-lobular LDs are an important source of fuel for BAT function and that chronic over activation of BAT impairs brown adipocyte survival.

The adrenergic stimulation of brown adipocyte thermogenesis initiated by cold exposure results in PKA activation, which activates mitochondrial fission, promotes enhanced uncoupling and sensitivity to fatty acids, thereby aiding heat generation [49]. BSCL2 deletion induces

cAMP/PKA signaling in BAT. When removed from the cellular or organismal context, isolated mitochondria from BKO BAT exhibited increased uncoupling, despite similar levels of UCP1 (Figure 4A, B). UCP1 has been shown to operate as an H^+ carrier activated by long-chain fatty acids (LCFAs) [57]. At present, we do not know whether UCP1 in mitochondria isolated from BSCL2-deleted BAT is more sensitive to LCFAs-stimulated uncoupling even in the presence of saturating levels of exogenous substrates. Alternatively, UCP1-independent mitochondrial uncoupling may be present in BKO BAT potentially through ADP/ATP exchange by the mitochondrial ADP/ATP carrier (AAC), as recently reported [58]. These possibilities will warrant future investigations. It is worth mentioning that the procedure of mitochondrial isolation by differential centrifugation may have selected healthy mitochondria and eliminated structurally deformed and dysfunctional mitochondria. Additionally, we were not able to identify a direct correlation of mitochondrial fragmentation with DRP1 phosphorylation and expression in BKO BAT (Fig. S3). In line with lack of mitophagic vesicles in BKO BAT under TEM, we also failed to observe altered protein expression of mitophagy/autophagy markers (P62 and LC3) in BAT of control and BKO mice housed at RT (Fig. S3), suggesting the accumulation of the fragmented mitochondria is not due to a failure in their clearance. Recent studies link mitochondrial dynamics to the balance between energy demand and nutrient supply [59,60]. Starvation has been shown to induce mitochondrial tubular network formation which protects mitochondria from autophagosomal degradation and supports cell viability [61,62]. We postulate that the heterogeneous mitochondrial shapes in BSCL2-deleted brown adipocytes in vivo may correlate with substrate availability and thus bioenergetic status. Ultimately, the exhaustion of fuel may lead to mitochondrial energetic collapse and dropout in cold exposed BKO BAT (Figure 5). Lastly, the ER may play a direct role in the process of mitochondrial fission [63]. We and others have demonstrated a close link between BSCL2 and mitochondrial metabolism ([33,40,42] and current study). Because BSCL2 is an ER protein, further studies are needed to test whether BSCL2 plays a direct role in regulating mitochondrial metabolism through mediating mitochondrial dynamics. In the current study, BKO BAT exhibited significant cellular and subcellular heterogeneity in response to thermogenic challenges, which raises the possibility that nutrient availability controls brown adipocyte mitochondrial dynamics and bioenergetics in vivo. Nevertheless, our data clearly show that BSCL2 deletion in BAT induces dynamic changes in mitochondrial shapes and function.

In general, BAT is known to be less prone to adipose tissue inflammation associated with obesity [64]. Interestingly, BAT-specific deletion of BSCL2 enhanced innate immune priming, particularly macrophages, which were greatly potentiated by cold exposure (Figure 3). Indeed, we observed recruitment of macrophages in BAT of BKO mice housed at both RT and 4 °C (Figure 3), but not at thermoneutrality (data not shown). Infiltration of pro-inflammatory M1 macrophages to BKO BAT may underlie impaired thermogenic capacity and reprograming by inhibiting the noradrenergic signaling that is essential for BAT recruitment and thermogenic function [65]. M2 macrophages have been shown to rapidly infiltrate BAT to release NE and sustain adaptive thermogenesis [66]. As such, increased infiltration of M2 macrophages in cold acclimated BKO BAT may be a compensatory response to defective noradrenergic signaling. Meanwhile, BAT fibrosis is positively correlated with inflammation, especially the expression of Galectin 3, an important fibrogenic factor whose inhibition prevents adipose tissue remodeling [67]. Unfortunately, inhibiting Galectin 3 by feeding mice with the pharmacological inhibitor of Galectin 3, modified citrus pectin (MCP; 100 mg kg^{-1} per day) in the drinking water was not able to rescue thermogenesis and reverse BAT pathological remodeling in BKO mice after cold acclimation (data not shown). Nevertheless, our data suggest that BSCL2 deletion in mature brown adipocytes causes BAT inflammation and fibrosis in response to a thermogenic challenge.

Adipocyte apoptotic death has been widely proposed as a key mechanism that leads to macrophage infiltration into adipose tissue [68—70]. Necroptosis is canonically initiated by the activation of Fas/CD95 or TNF receptor 1 (TNFR1) and usually initiates a more rapid and robust inflammatory responses than apoptosis [71]. It has been reported that obesity triggers RIPK3 overexpression in the WAT of mice and humans, where it dampens adipocyte apoptosis and inflammation to maintain WAT homeostasis [72]. The contribution of necroptosis to BAT remodeling has never been examined. Here, we, for the first time, identified brown adipocyte necroptosis that contributes to macrophage infiltration in BAT. The massive inflammation in BAT of cold-exposed or CL-injected BKO mice clearly highlights the involvement of necroptosis rather than apoptosis as a primary event leading to inflammation (Figures 5, 6). Surprisingly, BAT inflammation in BKO mice was not associated with significant upregulation of the principal pro-inflammatory chemokines (Figure 3). Physiologically, the stimulus/insult that initiates the necroptotic death pathway in BSCL2-deleted brown adipocytes remains unclear. Mitochondrial bioenergetic function is key to cell survival and in conditions of bioenergetic collapse, cells are diverted toward necrotic demise [73]. Notably, necroptosis has been associated with depolarized mitochondria and impaired ATP synthesis, which bypasses the canonical necroptosis pathway and is independent of TNF-α [52]. β-adrenergic signaling stimulates brown adipocyte mitochondrial fragmentation and depolarization [49]. Excessive β-adrenergic stimulated lipolysis has been linked to adipocyte death, although the manner of the specific cell death has not been defined [74]. We postulate that when BSCL2 deletion-induced lipolysis is accelerated by physiological and pharmacological β-adrenergic stimulation, it ultimately exhausts the supply of energy substrates, leading to mitochondrial bioenergetic collapse and thus necroptosis. Such a scenario could not be replicated in cultured *Bscl2*$^{-/-}$ brown adipocytes, preventing us from testing whether BAT-specific deletion of BSCL2 augments necroptosis in a brown adipocyte-specific manner. Considering that brown adipocytes comprise less than 55% of the cell population in BAT [75], we cannot exclude the possibility that the increased expression of necroptotic protein machinery may be derived from infiltrated immune cells. Unfortunately, brown adipocytes in BKO BAT were smaller with little or no LDs (Figure 4), prohibiting the fractionation of BAT into brown adipocytes and stromal vascular cell fractions for direct comparison. Nevertheless, TEM, the gold standard for the demarcation of different cell death modalities, confirmed the presence of necroptosis, especially in highly inflamed BKO BAT from mice exposed to chronic cold (Figure 5). These data underscore a novel brown adipocyte death pathway that contributes to BAT inflammation.

5. CONCLUSION

Our findings identify BSCL2 as a key player in regulating brown adipocyte function and turnover and highlight that fine-tuning of BAT cAMP/PKA activation to maintain energetic substrate availability may be crucial for optimizing adult BAT expansion, maintenance and thermogenic reprograming.

AUTHORS' CONTRIBUTION

W.C. conceived, designed, and supervised the project. H.Z. performed experiments and did data collection and analysis. C.X. performed

experiments. All authors interpreted and discussed. W.C. wrote and edited the manuscript.

ACKNOWLEDGMENTS

We sincerely thank Dr. Ruth Harris from Department of Physiology at Medical College of Georgia at Augusta University for proofreading the manuscript. We want to thank Augusta University Cancer Center Integrated Genomics Resource for RNA-sequencing analysis and Electron Microscopy and Histology Core for technical assistance and electron microscope imaging. This work was supported by the National Heart, Lung, and Blood Institute [1R01HL132182-01 to W.C.]; the American Heart Association Grant-in-aid [16GRNT30680004 to W.C.], and the American Heart Association Career Development Award (18CDA34080244 to H.Z.).

CONFLICT OF INTEREST

The authors declare no conflict of interest with any aspect of this article.

APPENDIX A. SUPPLEMENTARY DATA

Supplementary data to this article can be found online at https://doi.org/10.1016/j.molmet.2020.02.014.

REFERENCES

[1] Cannon, B., Nedergaard, J., 2004. Brown adipose tissue: function and physiological significance. Physiological Reviews 84(1):277—359.

[2] Saito, M., Okamatsu-Ogura, Y., Matsushita, M., Watanabe, K., Yoneshiro, T., Nio-Kobayashi, J., et al., 2009. High incidence of metabolically active brown adipose tissue in healthy adult humans: effects of cold exposure and adiposity. Diabetes 58(7):1526—1531.

[3] Yoneshiro, T., Aita, S., Matsushita, M., Okamatsu-Ogura, Y., Kameya, T., Kawai, Y., et al., 2011. Age-related decrease in cold-activated brown adipose tissue and accumulation of body fat in healthy humans. Obesity 19(9):1755—1760.

[4] Rothwell, N.J., Stock, M.J., 1983. Effects of age on diet-induced thermogenesis and brown adipose tissue metabolism in the rat. International Journal of Obesity 7(6):583—589.

[5] Lowell, B.B., V, S.S., Hamann, A., Lawitts, J.A., Himms-Hagen, J., Boyer, B.B., et al., 1993. Development of obesity in transgenic mice after genetic ablation of brown adipose tissue. Nature 366(6457):740—742.

[6] Bartelt, A., Bruns, O.T., Reimer, R., Hohenberg, H., Ittrich, H., Peldschus, K., et al., 2011. Brown adipose tissue activity controls triglyceride clearance. Nature Medicine 17(2):200—205.

[7] Cypess, A.M., Kahn, C.R., 2010. Brown fat as a therapy for obesity and diabetes. Current Opinion in Endocrinology, Diabetes, and Obesity 17(2):143—149.

[8] Hanssen, M.J., Hoeks, J., Brans, B., van der Lans, A.A., Schaart, G., van den Driessche, J.J., et al., 2015. Short-term cold acclimation improves insulin sensitivity in patients with type 2 diabetes mellitus. Nature Medicine 21(8):863—865.

[9] Yoneshiro, T., Aita, S., Matsushita, M., Kayahara, T., Kameya, T., Kawai, Y., et al., 2013. Recruited brown adipose tissue as an antiobesity agent in humans. The Journal of Clinical Investigation 123(8):3404—3408.

[10] Festuccia, W.T., Blanchard, P.G., Deshaies, Y., 2011. Control of brown adipose tissue glucose and lipid metabolism by PPARgamma. Frontiers in Endocrinology 2:84.

[11] Gonzalez-Hurtado, E., Lee, J., Choi, J., Wolfgang, M.J., 2018. Fatty acid oxidation is required for active and quiescent brown adipose tissue maintenance and thermogenic programing. Molecular Metabolism 7:45—56.

[12] Ellis, J.M., Li, L.O., Wu, P.C., Koves, T.R., Ilkayeva, O., Stevens, R.D., et al., 2010. Adipose acyl-CoA synthetase-1 directs fatty acids toward beta-oxidation and is required for cold thermogenesis. Cell Metabolism 12(1):53—64.

[13] Blondin, D.P., Frisch, F., Phoenix, S., Guerin, B., Turcotte, E.E., Haman, F., et al., 2017. Inhibition of intracellular triglyceride lipolysis suppresses cold-induced brown adipose tissue metabolism and increases shivering in humans. Cell Metabolism 25(2):438—447.

[14] Labbe, S.M., Caron, A., Bakan, I., Laplante, M., Carpentier, A.C., Lecomte, R., et al., 2015. In vivo measurement of energy substrate contribution to cold-induced brown adipose tissue thermogenesis. The FASEB Journal: Official Publication of the Federation of American Societies for Experimental Biology 29(5):2046—2058.

[15] Schreiber, R., Diwoky, C., Schoiswohl, G., Feiler, U., Wongsiriroj, N., Abdellatif, M., et al., 2017. Cold-induced thermogenesis depends on ATGL-mediated lipolysis in cardiac muscle, but not brown adipose tissue. Cell Metabolism 26(5):753—763 e757.

[16] Bronnikov, G., Bengtsson, T., Kramarova, L., Golozoubova, V., Cannon, B., Nedergaard, J., 1999. Beta1 to beta3 switch in control of cyclic adenosine monophosphate during brown adipocyte development explains distinct beta-adrenoceptor subtype mediation of proliferation and differentiation. Endocrinology 140(9):4185—4197.

[17] Davis, T.R., Johnston, D.R., Bell, F.C., Cremer, B.J., 1960. Regulation of shivering and non-shivering heat production during acclimation of rats. The American Journal of Physiology 198:471—475.

[18] Agarwal, A.K., Garg, A., 2004. Seipin: a mysterious protein. Trends in Molecular Medicine 10(9):440—444.

[19] Chen, W., Yechoor, V.K., Chang, B.H., Li, M.V., March, K.L., Chan, L., 2009. The human lipodystrophy gene product BSCL2/seipin plays a key role in adipocyte differentiation. Endocrinology 150(10):4552—4561.

[20] Magre, J., Delepine, M., Khallouf, E., Gedde-Dahl Jr., T., Van Maldergem, L., Sobel, E., et al., 2001. Identification of the gene altered in Berardinelli-Seip congenital lipodystrophy on chromosome 11q13. Nature Genetics 28(4):365—370.

[21] Payne, V.A., Grimsey, N., Tuthill, A., Virtue, S., Gray, S.L., Nora, E.D., et al., 2008. The human lipodystrophy gene BSCL2/seipin may be essential for normal adipocyte differentiation. Diabetes 57(8):2055—2060.

[22] Windpassinger, C., Auer-Grumbach, M., Irobi, J., Patel, H., Petek, E., Horl, G., et al., 2004. Heterozygous missense mutations in BSCL2 are associated with distal hereditary motor neuropathy and Silver syndrome. Nature Genetics 36(3):271—276.

[23] Chen, W., Chang, B., Saha, P., Hartig, S.M., Li, L., Reddy, V.T., et al., 2012. Berardinelli-Seip congenital lipodystrophy 2/seipin is a cell-autonomous regulator of lipolysis essential for adipocyte differentiation. Molecular and Cellular Biology 32(6):1099—1111.

[24] Cui, X., Wang, Y., Tang, Y., Liu, Y., Zhao, L., Deng, J., et al., 2011. Seipin ablation in mice results in severe generalized lipodystrophy. Human Molecular Genetics 20(15):3022—3030.

[25] Prieur, X., Dollet, L., Takahashi, M., Nemani, M., Pillot, B., Le May, C., et al., 2013. Thiazolidinediones partially reverse the metabolic disturbances observed in Bscl2/seipin-deficient mice. Diabetologia 56(8):1813—1825.

[26] Fei, W., Shui, G., Gaeta, B., Du, X., Kuerschner, L., Li, P., et al., 2008. Fld1p, a functional homologue of human seipin, regulates the size of lipid droplets in yeast. The Journal of Cell Biology 180(3):473—482.

[27] Romanauska, A., Kohler, A., 2018. The inner nuclear membrane is a metabolically active territory that generates nuclear lipid droplets. Cell 174(3):700—715 e718.

[28] Szymanski, K.M., Binns, D., Bartz, R., Grishin, N.V., Li, W.P., Agarwal, A.K., et al., 2007. The lipodystrophy protein seipin is found at endoplasmic reticulum lipid droplet junctions and is important for droplet morphology. Proc Natl Acad Sci U S A 104(52):20890—20895.

[29] Wang, S., Idrissi, F.Z., Hermansson, M., Grippa, A., Ejsing, C.S., Carvalho, P., 2018. Seipin and the membrane-shaping protein Pex30 cooperate in organelle budding from the endoplasmic reticulum. Nature Communications 9(1):2939.
[30] Wang, H., Becuwe, M., Housden, B.E., Chitraju, C., Porras, A.J., Graham, M.M., et al., 2016. Seipin is required for converting nascent to mature lipid droplets. Elife 5:e16582.
[31] Pagac, M., Cooper, D.E., Qi, Y., Lukmantara, I.E., Mak, H.Y., Wu, Z., et al., 2016. SEIPIN regulates lipid droplet expansion and adipocyte development by modulating the activity of glycerol-3-phosphate acyltransferase. Cell Reports 17(6):1546–1559.
[32] Bi, J., Wang, W., Liu, Z., Huang, X., Jiang, Q., Liu, G., et al., 2014. Seipin promotes adipose tissue fat storage through the ER Ca(2)(+)-ATPase SERCA. Cell Metabolism 19(5):861–871.
[33] Ding, L., Yang, X., Tian, H., Liang, J., Zhang, F., Wang, G., et al., 2018. Seipin regulates lipid homeostasis by ensuring calcium-dependent mitochondrial metabolism. The EMBO Journal 37(17):e97572.
[34] Yan, R., Qian, H., Lukmantara, I., Gao, M., Du, X., Yan, N., et al., 2018. Human SEIPIN binds anionic phospholipids. Developmental Cell 47(2):248–256 e244.
[35] Sui, X., Arlt, H., Brock, K.P., Lai, Z.W., DiMaio, F., Marks, D.S., et al., 2018. Cryo-electron microscopy structure of the lipid droplet-formation protein seipin. The Journal of Cell Biology 217(12):4080–4091.
[36] Talukder, M.M., Sim, M.F., O'Rahilly, S., Edwardson, J.M., Rochford, J.J., 2015. Seipin oligomers can interact directly with AGPAT2 and lipin 1, physically scaffolding critical regulators of adipogenesis. Molecular Metabolism 4(3):199–209.
[37] Sim, M.F., Dennis, R.J., Aubry, E.M., Ramanathan, N., Sembongi, H., Saudek, V., et al., 2012. The human lipodystrophy protein seipin is an ER membrane adaptor for the adipogenic PA phosphatase lipin 1. Molecular Metabolism 2(1):38–46.
[38] Castro, I.G., Eisenberg-Bord, M., Persiani, E., Rochford, J.J., Schuldiner, M., Bohnert, M., 2019. Promethin is a conserved seipin partner protein. Cells 8(3):268.
[39] Chung, J., Wu, X., Lambert, T.J., Lai, Z.W., Walther, T.C., Farese Jr., R.V., 2019. LDAF1 and seipin form a lipid droplet assembly complex. Developmental Cell 51(5):551–563 e557.
[40] Zhou, H., Lei, X., Benson, T., Mintz, J., Xu, X., Harris, R.B., et al., 2015. Berardinelli-Seip congenital lipodystrophy 2 regulates adipocyte lipolysis, browning, and energy balance in adult animals. Journal of Lipid Research 56(10):1912–1925.
[41] Dollet, L., Magre, J., Joubert, M., Le May, C., Ayer, A., Arnaud, L., et al., 2016. Seipin deficiency alters brown adipose tissue thermogenesis and insulin sensitivity in a non-cell autonomous mode. Scientific Reports 6:35487.
[42] Zhou, H., Black, S.M., Benson, T.W., Weintraub, N.L., Chen, W., 2016. Berardinelli-Seip congenital lipodystrophy 2/seipin is not required for brown adipogenesis but regulates Brown adipose tissue development and function. Molecular and Cellular Biology 36(15):2027–2038.
[43] Zhou, H., Lei, X., Yan, Y., Lydic, T., Li, J., Weintraub, N.L., et al., 2019. Targeting ATGL to rescue BSCL2 lipodystrophy and its associated cardiomyopathy. JCI Insight 4(14) e129781.
[44] Zheng, Q., Wang, X.J., 2008. GOEAST: a web-based software toolkit for gene ontology enrichment analysis. Nucleic Acids Research 36(Web Server issue): W358–W363.
[45] Chen, W., Zhou, H., Saha, P., Li, L., Chan, L., 2014. Molecular mechanisms underlying fasting modulated liver insulin sensitivity and metabolism in male lipodystrophic Bscl2/Seipin-deficient mice. Endocrinology 155(11):4215–4225.
[46] Vergnes, L., Davies, G.R., Lin, J.Y., Yeh, M.W., Livhits, M.J., Harari, A., et al., 2016. Adipocyte browning and higher mitochondrial function in periadrenal but not SC fat in pheochromocytoma. The Journal of Clinical Endocrinology and Metabolism 101(11):4440–4448.
[47] Kong, X., Banks, A., Liu, T., Kazak, L., Rao, R.R., Cohen, P., et al., 2014. IRF4 is a key thermogenic transcriptional partner of PGC-1alpha. Cell 158(1):69–83.
[48] Martinez-Santibanez, G., Singer, K., Cho, K.W., DelProposto, J.L., Mergian, T., Lumeng, C.N., 2015. Obesity-induced remodeling of the adipose tissue elastin network is independent of the metalloelastase MMP-12. Adipocyte 4(4):264–272.
[49] Wikstrom, J.D., Mahdaviani, K., Liesa, M., Sereda, S.B., Si, Y., Las, G., et al., 2014. Hormone-induced mitochondrial fission is utilized by brown adipocytes as an amplification pathway for energy expenditure. The EMBO Journal 33(5): 418–436.
[50] He, S., Wang, L., Miao, L., Wang, T., Du, F., Zhao, L., et al., 2009. Receptor interacting protein kinase-3 determines cellular necrotic response to TNF-alpha. Cell 137(6):1100–1111.
[51] Wang, H., Sun, L., Su, L., Rizo, J., Liu, L., Wang, L.F., et al., 2014. Mixed lineage kinase domain-like protein MLKL causes necrotic membrane disruption upon phosphorylation by RIP3. Mol Cell 54(1):133–146.
[52] Pajuelo, D., Gonzalez-Juarbe, N., Tak, U., Sun, J., Orihuela, C.J., Niederweis, M., 2018. NAD(+) depletion triggers macrophage necroptosis, a cell death pathway exploited by Mycobacterium tuberculosis. Cell Reports 24(2):429–440.
[53] Harms, M., Seale, P., 2013. Brown and beige fat: development, function and therapeutic potential. Nature Medicine 19(10):1252–1263.
[54] Sanchez-Gurmaches, J., Hung, C.M., Sparks, C.A., Tang, Y., Li, H., Guertin, D.A., 2012. PTEN loss in the Myf5 lineage redistributes body fat and reveals subsets of white adipocytes that arise from Myf5 precursors. Cell Metabolism 16(3):348–362.
[55] Han, Y.H., Buffolo, M., Pires, K.M., Pei, S., Scherer, P.E., Boudina, S., 2016. Adipocyte-specific deletion of manganese superoxide dismutase protects from diet-induced obesity through increased mitochondrial uncoupling and biogenesis. Diabetes 65(9):2639–2651.
[56] Stefl, B., Janovska, A., Hodny, Z., Rossmeisl, M., Horakova, M., Syrovy, I., et al., 1998. Brown fat is essential for cold-induced thermogenesis but not for obesity resistance in aP2-Ucp mice. The American Journal of Physiology 274(3 Pt 1):E527–E533.
[57] Fedorenko, A., Lishko, P.V., Kirichok, Y., 2012. Mechanism of fatty-acid-dependent UCP1 uncoupling in brown fat mitochondria. Cell 151(2):400–413.
[58] Bertholet, A.M., Chouchani, E.T., Kazak, L., Angelin, A., Fedorenko, A., Long, J.Z., et al., 2019. H(+) transport is an integral function of the mitochondrial ADP/ATP carrier. Nature 571(7766):515–520.
[59] Liesa, M., Shirihai, O.S., 2013. Mitochondrial dynamics in the regulation of nutrient utilization and energy expenditure. Cell Metabolism 17(4):491–506.
[60] Mishra, P., Chan, D.C., 2016. Metabolic regulation of mitochondrial dynamics. The Journal of Cell Biology 212(4):379–387.
[61] Gomes, L.C., Di Benedetto, G., Scorrano, L., 2011. During autophagy mitochondria elongate, are spared from degradation and sustain cell viability. Nature Cell Biology 13(5):589–598.
[62] Rambold, A.S., Kostelecky, B., Elia, N., Lippincott-Schwartz, J., 2011. Tubular network formation protects mitochondria from autophagosomal degradation during nutrient starvation. Proc Natl Acad Sci U S A 108(25):10190–10195.
[63] Friedman, J.R., Lackner, L.L., West, M., DiBenedetto, J.R., Nunnari, J., Voeltz, G.K., 2011. ER tubules mark sites of mitochondrial division. Science 334(6054):358–362.
[64] Fitzgibbons, T.P., Kogan, S., Aouadi, M., Hendricks, G.M., Straubhaar, J., Czech, M.P., 2011. Similarity of mouse perivascular and brown adipose tissues and their resistance to diet-induced inflammation. American Journal of Physiology Heart and Circulatory Physiology 301(4):H1425–H1437.
[65] Sakamoto, T., Nitta, T., Maruno, K., Yeh, Y.S., Kuwata, H., Tomita, K., et al., 2016. Macrophage infiltration into obese adipose tissues suppresses the induction of UCP1 level in mice. American Journal of Physiology Endocrinology and Metabolism 310(8):E676–E687.
[66] Nguyen, K.D., Qiu, Y., Cui, X., Goh, Y.P., Mwangi, J., David, T., et al., 2011. Alternatively activated macrophages produce catecholamines to sustain adaptive thermogenesis. Nature 480(7375):104–108.

[67] Martinez-Martinez, E., Calvier, L., Rossignol, P., Rousseau, E., Fernandez-Celis, A., Jurado-Lopez, R., et al., 2016. Galectin-3 inhibition prevents adipose tissue remodelling in obesity. International Journal of Obesity 40(6):1034—1038.

[68] Alkhouri, N., Gornicka, A., Berk, M.P., Thapaliya, S., Dixon, L.J., Kashyap, S., et al., 2010. Adipocyte apoptosis, a link between obesity, insulin resistance, and hepatic steatosis. Journal of Biological Chemistry 285(5):3428—3438.

[69] Cinti, S., Mitchell, G., Barbatelli, G., Murano, I., Ceresi, E., Faloia, E., et al., 2005. Adipocyte death defines macrophage localization and function in adipose tissue of obese mice and humans. Journal of Lipid Research 46(11): 2347—2355.

[70] Pajvani, U.B., Trujillo, M.E., Combs, T.P., Iyengar, P., Jelicks, L., Roth, K.A., et al., 2005. Fat apoptosis through targeted activation of caspase 8: a new mouse model of inducible and reversible lipoatrophy. Nature Medicine 11(7):797—803.

[71] Newton, K., Manning, G., 2016. Necroptosis and inflammation. Annual Review of Biochemistry 85:743—763.

[72] Gautheron, J., Vucur, M., Schneider, A.T., Severi, I., Roderburg, C., Roy, S., et al., 2016. The necroptosis-inducing kinase RIPK3 dampens adipose tissue inflammation and glucose intolerance. Nature Communications 7:11869.

[73] Kushnareva, Y., Newmeyer, D.D., 2010. Bioenergetics and cell death. Annals of the New York Academy of Sciences 1201:50—57.

[74] Lee, Y.H., Petkova, A.P., Granneman, J.G., 2013. Identification of an adipogenic niche for adipose tissue remodeling and restoration. Cell Metabolism 18(3):355—367.

[75] Rosenwald, M., Perdikari, A., Rulicke, T., Wolfrum, C., 2013. Bi-directional interconversion of brite and white adipocytes. Nature Cell Biology 15(6):659—667.

